J. Fluid Mech. (1976), *vol.* 76, *part* 4, *pp.* 653–674
Printed in Great Britain

Rolling motion of a sphere on a plane boundary in oscillatory flow

By C. SAMUEL MARTIN, M. PADMANABHAN
School of Civil Engineering, Georgia Institute of Technology, Atlanta

AND C. D. PONCE-CAMPOS
University of Michigan, Ann Arbor

(Received 19 November 1975)

The rolling motion of a sphere on a smooth plane boundary in a simple-harmonic water motion has been analytically and experimentally investigated. For spheres having specific gravities ranging from 0·09 to 15·18 the sphere motion was found to be sinusoidal for both low and high values of the period parameter defined by Keulegan & Carpenter. The knowledge of the sphere motion, and hence the resultant force, allowed the determination of inertia and drag coefficients from Fourier-averaging techniques. Experiments in the inertial range yielded an added-mass coefficient of 1·2, compared with 0·67 from inviscid theory for translating spheres. For values of the period parameter greater than 30 the drag coefficient is reported to be approximately 0·74.

1. Introduction

There is limited experimental and theoretical information available on the hydrodynamic forces on objects adjacent to a boundary in either steady or unsteady flow. The pressure distribution and the attendant resistance forces, lift and drag, are the principal desired quantities for steady flow past objects on or in close proximity to a boundary. Unsteady flow situations, whether transient, pulsatile or oscillatory, require the determination of the inertial effects in addition to those of resistance. Furthermore, unsteady flows can generate an additional force that is related to the history of the motion, whether transient or oscillatory.

It is of interest to have a knowledge of the hydrodynamic forces when assessing the fluid forces on sediment particles on a beach under shoaling waves, as reported by Eagleson & Dean (1961), or in the design of structures to be placed on the sea bottom. Other applications with or without boundary effects are the influence of pulsating flow on gas absorption in liquids, liquid–liquid extraction (Al-Taweel & Carley 1971), and vertical retardation of suspensions in tubes (Tunstall & Houghton 1968). The only known previous investigation of the rolling motion of spheres was conducted by Chan, Baird & Round (1974), who were prompted to do the studies to gain more knowledge on the transport of dense solids in conduits by the pulsatile flow of liquids.

1.1. *Steady flow*

The influence of a boundary on the steady fluid motion around spheres near a wall has been investigated analytically for very slow motion by Landenburg (1907), Faxén (1921) and McNown *et al.* (1948). More recently, the case of a sphere rotating parallel to a nearby plane wall in an otherwise still fluid was solved analytically for Stokes flow by Dean & O'Neill (1963). O'Neill (1964) also solved the equations for the related problem of a translating sphere. Goldman, Cox & Brenner (1967) attempted to approach the limiting case of a rotating sphere on a plane wall, but found that the sphere could not actually be in direct contact with the boundary, resulting in an actual slip. Over a range of Reynolds numbers, Carty (1957), whose results are also reported in Eagleson & Dean (1961), measured the terminal velocity of spheres rolling down a plane boundary, providing the experimental values for a drag coefficient for rotating spheres on a plane boundary. Later Chan *et al.* (1974) conducted similar experiments in a conduit.

1.2. *Transient motion*

For the rectilinear transient motion of spheres the pioneering work by Basset (1910) for low Reynolds number flows proved that there exists a history term in addition to the inertia or so-called added-mass term. The influence of the history term and the validity of Basset's theory has been verified by Brush, Ho & Yen (1964), Hjelmfelt & Mockros (1967), Mockros & Lai (1969), Waugh & Ellis (1969) and Hamilton & Lindell (1971). It has not been clearly established, however, that the history term as defined by Basset is valid for large Reynolds numbers in transient flows, or oscillatory flows.

1.3. *Oscillatory motion*

Stokes (1851) integrated the Navier–Stokes equations to determine the viscous and inertia effects on oscillating spheres in an infinite and otherwise quiescent fluid. Wagenschein (1921) and Carstens (1952) experimentally corroborated Stokes' theory in its range of validity. In an unconfined medium the inertia and drag coefficients have been measured on a stationary sphere by Sarpkaya (1975) for higher Reynolds numbers. For the case of a sinusoidally oscillating sphere in a viscous liquid, Odar & Hamilton (1964) determined the history coefficient as well as the inertia coefficient. Upward pulsatile flows and the attendant suspension of solid particles have been investigated by Al-Taweel & Carley (1971) and Tunstall & Houghton (1968). The radial migration of suspensions in oscillatory flow in horizontal tubes was demonstrated by Shizgal, Goldsmith & Mason (1965). For spheres resting on a boundary, attempts at the determination of the drag and inertia coefficients have been made by O'Brien & Morison (1952), Grace & Casciano (1969) and Garrison & Berklite (1973). The latter researchers experimentally and analytically determined the effect of the wall on the inertia or added-mass coefficients for high frequencies of oscillation. Although there have been numerous investigations on the hydrodynamics of oscillatory flow around rounded bodies, and limited attention to boundary proximity effects, the designer still experiences considerable difficulty in estimating forces on bodies in unsteady flow.

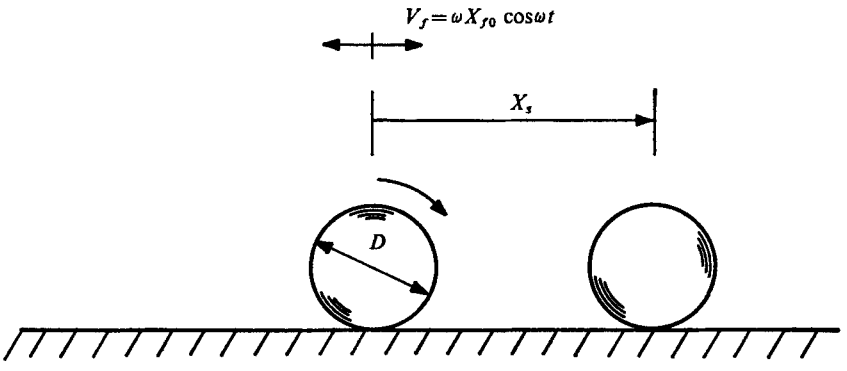

FIGURE 1. Definition sketch of sphere on boundary.

This paper is concerned with the determination of the fluid forces, inertia and drag on spheres on a plane boundary in an oscillatory flow. A definition sketch of the sphere and fluid is provided by figure 1.

2. Experimental equipment

2.1. U-*tube*

All of the experimental data reported here were obtained using a large U-tube, a photograph of which is shown in figure 2 (plate 1). Simple-harmonic water motion at the natural frequency of the system is produced by a feedback-control system. The flow passage in the test section B in figure 3 is 0·305 m high and 1·21 m wide. The free-surface dimensions in each vertical leg are identical to those in the test section. Although a sand bed D is depicted in figure 3, a smooth aluminium plate constituted the entire floor of the test section for the rolling ball tests. Visual observation of any phenomena within the test section is possible by virtue of the transparent walls and top of the horizontal test section. Area C is simply a solid region bounded by streamlined plates.

The system is designed to oscillate at various amplitudes at the resonant system frequency. Through conduit J a continuous supply of air from a variable-speed centrifugal blower supplies the pressure to force the corresponding water surface downward whenever the solenoid-operated exhaust valves E are closed. These exhaust valves are open while the water surface in that tank is rising, allowing for a short circuit of air from the conduit back through the valves. The phasing of valves E is controlled by a float F on the other water surface, and a direction-sensing switch H which actuates a timing circuit.

An instantaneous record of the position of the steel rod G and the attached float F is determined by means of a linear-variable – differential – transformer, which is mechanically connected by wires and pulleys to the rod and cable system. The amplitude and period of oscillation were recorded on a direct-writing oscillograph. The natural period of the U-tube is 3·56 s. By changing the blower speed the water displacement in the test section can be continuously varied from 0 to 75 cm.

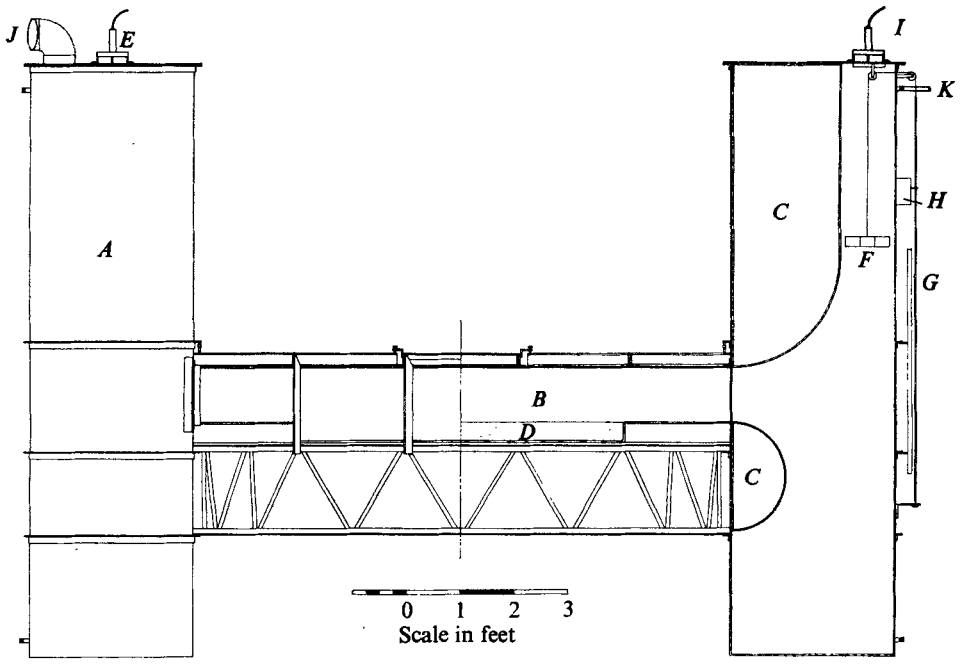

FIGURE 3. Cross-section of U-tube. *A*, steel tanks; *B*, test section; *C*, streamlined inserts; *D*, sand bed; *E*, exhaust valve; *F*, float; *G*, steel rod; *H*, direction-sensing switch; *I*, blow-down and damping valve; *J*, air supply (1); *K*, air supply (2).

Two methods have been used to ascertain the actual nature of the oscillatory water motion in the test facility. After construction of the facility, free oscillation tests were conducted to obtain the effective mass and the damping coefficient of the U-tube. Below an amplitude of 25 cm the damping is definitely linear, resulting in a value of the logarithmic decrement of approximately 0·09. For an assumed forced air pressure input represented by a rectified square wave, a Fourier series solution to the calibrated differential equation yielded no harmonic more than 0·1% of the fundamental amplitude of the water motion. A harmonic analysis of the steady-state motion of neutrally buoyant particles in the middle of the test section confirmed the analytical predictions, yielding all other harmonics with amplitudes less than 1%. The boundary layer on the floor of the test section was observed to be laminar for the amplitudes of motion employed in these tests. For the fixed frequency of oscillation of the water motion and a representative water temperature the thickness of the so-called depth of penetration of the oscillating Stokes layer is approximately 0·1 cm from $(2\nu/\omega)^{\frac{1}{2}}$, where ν is the kinematic fluid viscosity and ω the angular frequency.

2.2. *Sphere characteristics*

Sixteen different balls having specific gravities ranging from 0·09 (ping-pong) to 15·18 (tungsten carbide steel) were used as the test spheres. As shown in table 1 the magnitude of sphere diameters varied from 0·794 cm to 5·636 cm. The commercial ceramic and metal balls possessed a very high degree of roundness.

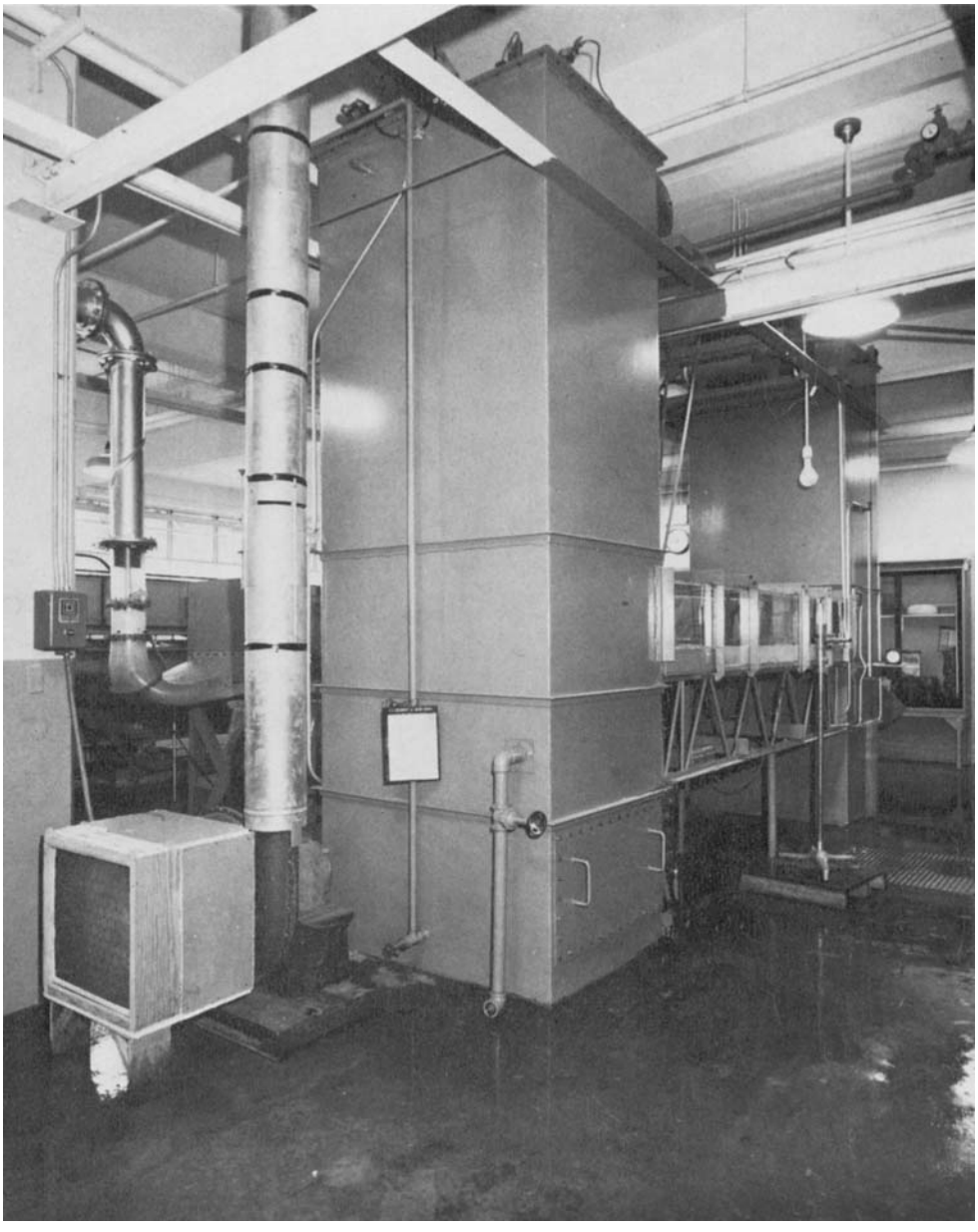

FIGURE 2. View of U-tube.

TABLE 1. Summary of experimental results

Run	Material	Specific gravity	D (cm)	X_{f0}/D	X_{s0}/D	ϕ (deg)	Stokes number $\omega D^2/\nu$	Reynolds number $\omega\lvert X_{f0}-X_{s0}\rvert D/\nu$	Period parameter $2\pi\lvert X_{f0}-X_{s0}\rvert/D$
1	Glass	2·47	2·489	3·06	1·56	11·7	1173	1795	9·4
2				6·12	3·55	21·7		3100	16·2
3				9·18	6·02	17·5		3850	19·9
4	Blue glass	2·54	2·235	3·41	1·76	10·2	946	1560	10·4
5				6·82	4·01	25·9		2660	17·7
6				10·23	6·68	21·3		3360	22·3
7	Nylon I	1·16	2·540	3·00	2·33	0·4	1222	820	4·2
8				6·00	4·80	8·0		1470	7·5
9				9·00	7·47	8·3		1870	9·6
10	Nylon II	1·41	2·540	3·00	2·06	1·3	1222	1150	5·9
11				6·00	4·49	10·9		1850	9·5
12				9·00	7·06	9·5		2370	12·2
13	Plastic	1·19	2·540	3·00	2·29	2·0	1222	870	4·5
14				6·00	4·76	4·8		1520	7·8
15				9·00	7·43	5·5		1920	9·9
16	Billiard ball	1·93	5·636	1·35	0·66	3·5	6015	4160	4·3
17				2·70	1·50	20·5		7220	7·5
18				4·05	2·58	21·5		8840	9·2
19	Stainless steel	7·73	2·540	3·00	0·63	15·7	1222	2900	14·9
20				6·00	1·71	34·8		5240	27·0
21				9·00	2·96	41·7		7380	38·0
22			1·905	4·00	0·92	20·3	687	2120	19·4
23				8·00	2·45	40·2		3810	34·9
24				12·00	4·48	45·8		5170	47·3
25			1·588	4·80	1·18	26·9	477	1730	22·7
26				9·60	3·30	35·4		3010	39·6
27				14·40	6·03	40·0		3990	52·6

TABLE 1 (*cont.*)

Run	Material	Specific gravity	D (cm)	X_{f0}/D	X_{s0}/D	ϕ (deg)	Stokes number $\omega D^2/\nu$	Reynolds number $\omega\lvert X_{f0}-X_{s0}\rvert D/\nu$	Period parameter $2\pi\lvert X_{f0}-X_{s0}\rvert/D$
28			1·270	6·00	1·50	11·9	305	1370	28·3
29				12·00	4·46	36·7		2300	47·4
30				18·00	8·16	37·9		3000	61·8
31			1·111	6·86	1·81	17·9	234	1180	31·7
32				13·72	5·51	33·5		1920	51·6
33				20·58	10·26	39·0		2420	64·8
34			0·794	9·60	3·55	20·1	119	720	38·0
35				19·20	8·61	25·9		1260	66·5
36				28·80	16·03	27·5		1520	80·2
37	Ping-pong	0·09	3·731	3·27	4·08	—	2636	2140	5·1
38				4·56	5·62	—		2790	6·7
39				8·16	8·95	—		2080	5·0
40				8·85	9·87	—		2690	6·4
41	Ceramic	3·95	2·540	3·00	0·84	—	1222	2210	11·4
42				5·00	1·85	—		3510	18·1
43				6·00	2·50	—		4070	21·0
44				8·00	3·52	—		5080	26·2
45				9·00	4·31	—		5490	28·3
46				11·00	5·76	—		6240	32·2
47	Hasteloy steel	8·89	2·540	6·00	1·35	—	1222	5660	29·2
48				9·00	2·67	—		7720	39·8
49				12·00	3·90	—		9870	50·9
50				13·00	4·70	—		10120	52·2
51				15·00	5·57	—		11500	59·3
52	Tungsten carbide steel	15·18	2·540	9·00	1·74	—	1222	8840	45·6
53				11·00	2·43	—		10430	53·8
54				13·00	3·33	—		11790	60·8
55				16·00	4·48	—		14040	72·4

2.3. *Test procedure*

For the purpose of establishing a reference scale within the test section a thin transparent sheet of plastic with closely spaced dark lines was stretched tightly on part of the test section floor. Before each series of tests with an individual sphere the U-tube was emptied and a cover on the top of the test section was lifted off, allowing the test sphere to be placed on the aluminium floor. The air blower speed was preset to produce a steady-state amplitude of water displacement. Once steady-state conditions were attained the amplitude of the water motion X_{f0} was visually observed from the motion of the rod G. The amplitude of the displacement of the centre of the sphere X_{s0} was obtained by using the reference lines on the adjacent plastic sheet. The ping-pong ball, which oscillated under the cover of the test section, was observed through the transparent top.

In some tests motion pictures of the rod motion and the sphere motion were taken. An incandescent light connected to the direction-sensing switch H allowed determination of the change in direction of the water. Independent filming of ball motion and rod motion with this light in view, which was off during one-half of the cycle and on during the remaining portion, provided for the measurement of the phase angle ϕ.

A total of 55 runs were conducted using the 16 different spheres. Table 1 provides a summary of the data in terms of the dimensionless parameters X_{f0}/D and X_{s0}/D, and the phase angle ϕ. Only for those 36 runs for which motion pictures were taken are values of ϕ available. As discussed later the values of ϕ in table 1 were determined by performing a harmonic analysis of both the water motion and sphere motion records.

3. Experimental results

3.1. *Dimensionless parameters*

We employ dimensional analysis to formulate representative parameters for correlating the two measured quantities, X_{s0} and ϕ, with the fluid properties, sphere characteristics and flow characteristics. The amplitude of sphere displacement X_{s0} can be expressed as follows:

$$X_{s0} = f[X_{f0}, D, \omega, \nu, \rho_f, \rho_s], \tag{3.1}$$

where X_{f0} is the amplitude of fluid displacement, D the sphere diameter, ρ_f the mass density of the fluid and ρ_s the mass density of the sphere. One possible combination of dimensionless parameters is

$$\frac{X_{s0}}{D} = f\left[\frac{X_{f0}}{D}, \frac{\omega(X_{f0}-X_{s0})D}{\nu}, \frac{\rho_s}{\rho_f}\right]. \tag{3.2}$$

Defining V_{f0} and V_{s0} as the respective amplitudes of the fluid and sphere velocities,

$$R = \frac{\omega|X_{f0}-X_{s0}|D}{\nu} = \frac{|V_{f0}-V_{s0}|D}{\nu} \tag{3.3}$$

is referred to as a translational Reynolds number by Happel & Brenner (1965).

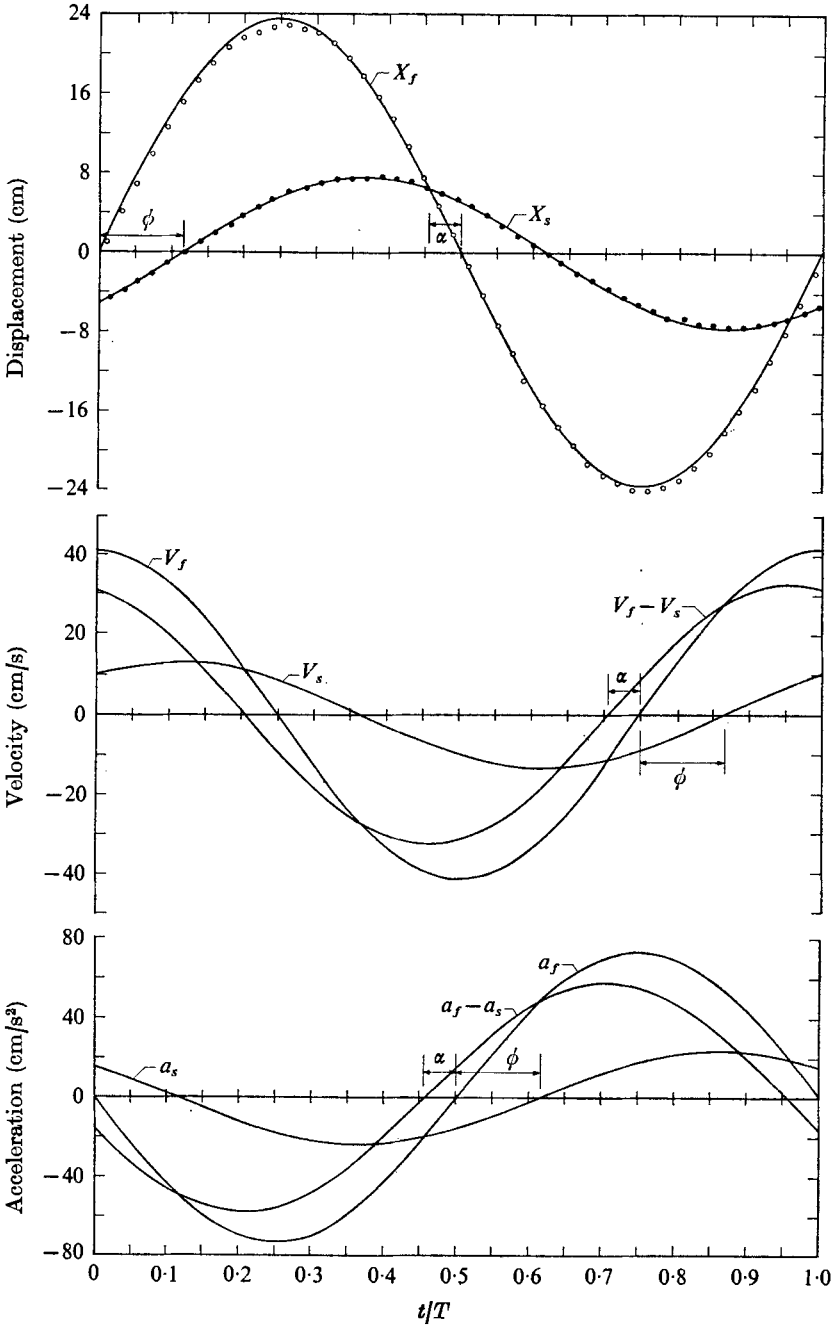

FIGURE 4. Kinematical properties of fluid and sphere motion: ○, measured values of X_f; ●, measured values of X_s; ————, fundamental from harmonic analysis.

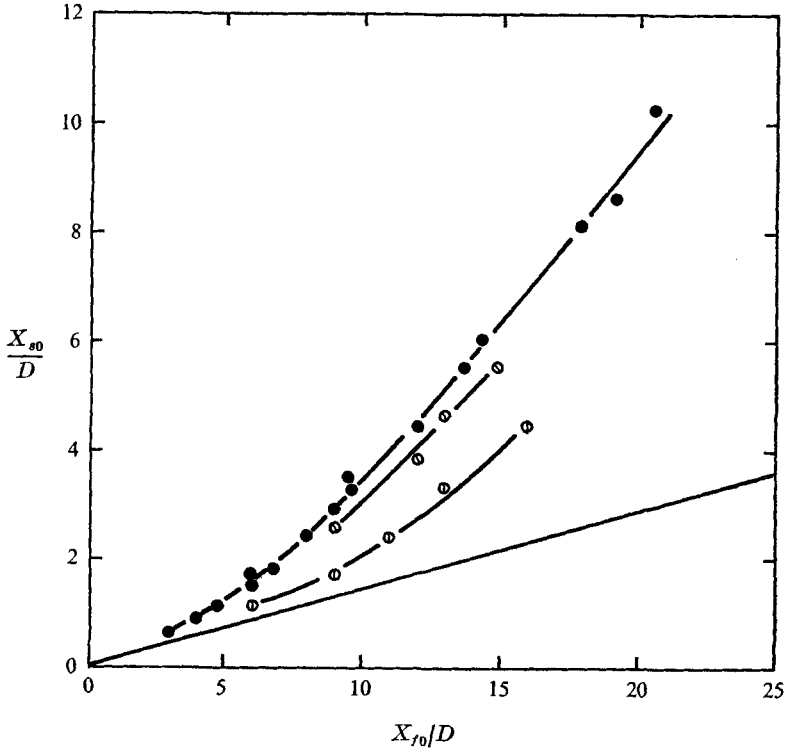

FIGURE 5. Sphere amplitude *vs.* fluid amplitude for metal spheres: —— —— ——, best-fit curve through data; ———, inviscid theory, $C_M = 0{\cdot}67$, $\rho_r = 7{\cdot}73$. Data: ●, $\rho_r = 7{\cdot}73$; ⊘, $\rho_r = 8{\cdot}89$; ⓘ, $\rho_r = 15{\cdot}18$.

The absolute-value sign is employed to preclude the presence of a negative Reynolds number in the event that $X_{s0} > X_{f0}$. Another choice of dimensionless ratios might be

$$\frac{X_{f0}-X_{s0}}{D} = f\left[\frac{X_{f0}}{D}, \frac{\omega D^2}{\nu}, \rho_r\right], \tag{3.4}$$

where $\rho_r = \rho_s/\rho_f$ and

$$S = \omega D^2/\nu \tag{3.5}$$

is an occasionally used form of Stokes number, or a rotational Reynolds number according to Happel & Brenner (1965). The dependent quantity in (3.4) is related to what is frequently called the period parameter (Keulegan & Carpenter 1958):

$$P = |V_{f0}-V_{s0}|\,T/D = 2\pi|X_{f0}-X_{s0}|/D, \tag{3.6}$$

where T is the period of the oscillation. Numerical values of the two Reynolds numbers and the period parameter are listed in table 1 for all the runs.

3.2. *Analysis of form of motion*

For all tests for which motion pictures were taken a detailed analysis of both the water motion and the sphere motion was possible. A total of 48 intervals per cycle of oscillation were chosen to reduce the data. A harmonic analysis of both motions

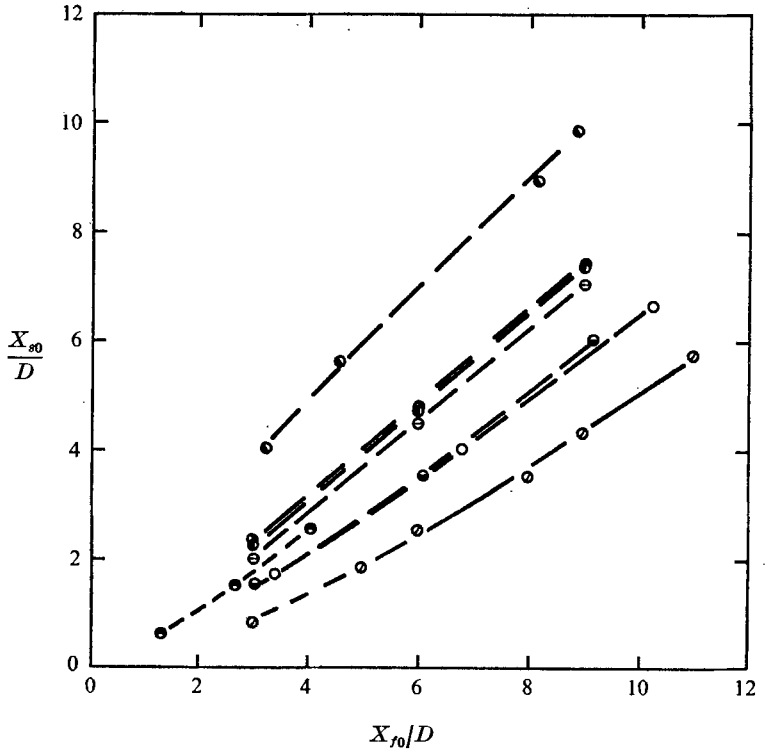

FIGURE 6. Sphere amplitude *vs.* fluid amplitude for other spheres: —— —— ——, best-fit curve through data. ρ_r: ◔, 0·09; ◑, 1·16; ◐, 1·19; ⊖, 1·41; ◓, 1·93; ◒, 2·47; ○, 2·54; ⊘, 3·95.

provided information on the amplitude, phase and form of the respective displacements. A representative sample of the actual motion is depicted on figure 4 for run 21, the 2·54 cm stainless-steel sphere in a water motion corresponding to $X_{f0} = 22{\cdot}9$ cm. The data points are the actual values of X_f and X_s reduced from the motion pictures. Both the water motion and the sphere motion were found to be very close to sinusoidal by a Fourier analysis. The amplitude and phase of the fundamental sphere motion ascertained from the harmonic analysis compared favourably with the values calculated from visual observations.

Assuming the motion to be simple harmonic the other kinematic characteristics of the sphere motion, V_s and a_s, were calculated accordingly and plotted on figure 4. The velocity difference $V_f - V_s$ is also included to demonstrate that the relative velocity, and the drag force, actually lead the water velocity V_f.

3.3. *Sphere amplitude*

The ratio of sphere displacement to its diameter X_{s0}/D is correlated with the ratio X_{f0}/D for various density ratios ρ_r in figure 5 for metal spheres, and in figure 6 for the remaining ones. The Stokes number, which ranged from 119 to 6015, could not be correlated with the results, probably because it lies within the inertial range. This independence of the motion of the Stokes number is fairly

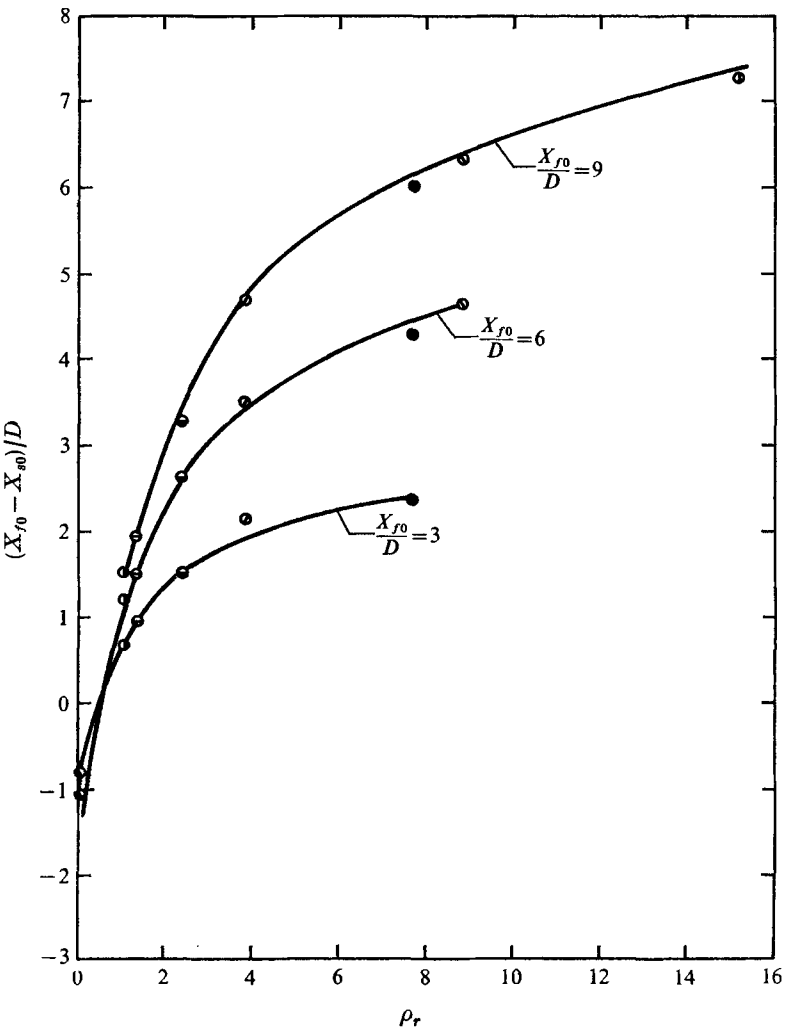

FIGURE 7. Correlation of amplitude data with density ratio: ———, Runge–Kutta numerical integration. ρ_r: ◔, 0·09; ◑, 1·16; ◐, 1·19; ⊖, 1·41; ◒, 2·47; ⊘, 2·54; ●, 3·95; ⊗, 8·89; ⊙, 15·18.

obvious upon inspection of the results in figure 5 for the stainless-steel spheres For values of X_{f0}/D of 6, 9·6 and 12 the ratios X_{s0}/D are nearly equal for corresponding Stokes numbers of 305 and 1222, 119 and 477, and 305 and 687, respectively. Except for the lower range of the translational Reynolds number R, which varied from 720 to 14040, there is apparently no Reynolds number effect on the amplitude of sphere motions either.

The effect of the mass density of the respective spheres is clearly shown in figures 5 and 6. For a given water motion and sphere diameter the denser balls experience a greater relative velocity and acceleration than the lighter ones. Clearly, as shown by the kinematical representation offigure 4, the fluid resistance force alternates from a motivating force to a retarding force during the cycle. The

correlation of the amplitude results with the density ratio is possible for constant values of X_{f0}/D, as shown in figure 7 in terms of $(X_{f0}-X_{s0})/D$ *vs.* ρ_r for values of $X_{f0}/D = 3$, 6 and 9.

4. Theory

We assume that the sphere shown on the plane boundary on figure 1 is immersed in a sinusoidally oscillating fluid and is allowed to roll. The equation of linear momentum is

$$F_P + F_D + F_M + F_H - F_R = M_s a_s, \tag{4.1}$$

where F_P is the pressure force associated with the pressure gradient required to oscillate the fluid, and F_D is the horizontal component of the fluid resistance force, the so-called drag force. The term associated with the relative acceleration between the fluid and body is the added-mass or inertia force F_M. The other two forces are the rolling friction F_R and the force related to the history of the fluid motion F_H. Representing the inertia of the sphere is M_s, its mass, and a_s, the instantaneous linear sphere acceleration.

Actually, the rolling friction force can be eliminated from the analysis if the law of angular momentum is employed. If $F_H = 0$ and the sphere is assumed to roll without sliding, the angular momentum equation about an axis through the centre of gravity of the sphere shown in figure 1 can be expressed as

$$\tfrac{1}{2}DF_R + (l_D - \tfrac{1}{2}D)\,F_D + (l_M - \tfrac{1}{2}D)\,F_M = \frac{d}{dt}\int_{\mathscr{V}} r^2\omega\, dM_s, \tag{4.2}$$

where l_D and l_M are the location of the lines of action of the drag and inertia forces, respectively. We have assumed that the pressure force is applied through the axis of the sphere. The right-hand side of (4.2) is simply

$$\frac{d}{dt}\int_{\mathscr{V}} r^2\omega\, dM_s = \frac{2}{5}\frac{D}{2}M_s a_s. \tag{4.3}$$

Using (4.2) and (4.3) we solve for F_R and substitute the result into (4.1), resulting in the relationship

$$F_P + \frac{2l_D}{D}F_D + \frac{2l_M}{D}F_M = \tfrac{7}{5}M_s a_s. \tag{4.4}$$

Although the difficulty in evaluating the force of rolling friction has been eliminated, (4.4) is intractable because of the unknown values of the lines of action l_M and l_D of the two forces F_M and F_D. Equation (4.4) differs from (4.1) by the coefficients of F_D and F_M and the effect of the rotating inertia of the rolling sphere itself, as represented by $\frac{7}{5}M_s a_s$. The fluid inertia term can actually be referred to as a rotational fluid inertia or rotational added mass. Since l_D and l_M are not easily determined they are set equal to $\frac{1}{2}D$ in (4.4) for convenience, resulting in

$$F_P + F_D + F_M = \tfrac{7}{5}M_s a_s. \tag{4.5}$$

Equation (4.5) differs from (4.1) by the absence of F_R, which was eliminated, by the fact that F_H was neglected, and by the inclusion of the rotating inertia of

the sphere itself. Moreover, the terms F_D and F_M include the effect of the respective moments of fluid drag and fluid inertia. Because of the form of F_D and F_M in (4.5) the respective coefficients of drag C_D and inertia C_M embody these effects. Chan *et al.* (1974) begin with an expression similar to (4.5) by adding to (4.1) the rotational inertia term, which is $\frac{2}{5}$ of the sphere mass times linear acceleration.

Neglecting the influence of the wall boundary layer, which was in all cases considerably smaller in height than the sphere diameter, we define the kinematic properties of the fluid motion by

$$X_f = X_{f0} \sin \omega t, \tag{4.6}$$

where t is the time. The fluid velocity becomes

$$V_f = dX_f/dt = \omega X_{f0} \cos \omega t, \tag{4.7}$$

and the acceleration $$a_f = dV_f/dt = -\omega^2 X_{f0} \sin \omega t. \tag{4.8}$$

We represent the motion of the centre of mass of the sphere by X_s for displacement, V_s for velocity and a_s for acceleration.

In the absence of a wall boundary layer the pressure force is simply equal to the mass of displaced fluid M_f times the fluid acceleration. Equation (4.5) can then be expressed as

$$M_f a_f + C_M M_f (a_f - a_s) + \tfrac{1}{2}\rho_f C_D \tfrac{1}{4}\pi D^2 (V_f - V_s)\,|V_f - V_s| = \tfrac{7}{5} M_s a_s, \tag{4.9}$$

in which C_D and C_M are the effective drag and added-mass coefficients, respectively, for forces on a rotating sphere. The moment arms defined in (4.4) are lumped in C_D and C_M. Equation (4.9) can be written in terms of the unknown sphere displacement X_s as

$$-\omega^2 X_{f0} \sin \omega t - C_M\left(\omega^2 X_{f0} \sin \omega t + \frac{d^2 X_s}{dt^2}\right) + \tfrac{3}{4}\frac{C_D}{D}\left(\omega X_{f0} \cos \omega t - \frac{dX_s}{dt}\right)$$
$$\left|\omega X_{f0} \cos \omega t - \frac{dX_s}{dt}\right| = \tfrac{7}{5}\frac{\rho_s}{\rho_f}\frac{d^2 X_s}{dt^2}. \tag{4.10}$$

4.1. *Stokes flow*

For slow motion, for which

$$C_D = \frac{K\nu}{D(V_f - V_s)}, \tag{4.11}$$

equation (4.10) was apparently originally solved by König (1891). For this linear differential equation the resulting steady-state sphere motion is also sinusoidal:

$$\frac{X_s}{X_{f0}} = \left[\frac{(1+C_M)^2 + \beta^2}{(\frac{7}{5}\rho_r + C_M)^2 + \beta^2}\right]^{\frac{1}{2}} \sin(\omega t - \phi), \tag{4.12}$$

where $\rho_r = \rho_s/\rho_f$ is the density ratio. The phase lag between sphere and fluid motion is

$$\tan \phi = \frac{\beta(\frac{7}{5}\rho_r - 1)}{(\frac{7}{5}\rho_r + C_M)(1 + C_M) + \beta^2}, \tag{4.13}$$

where $$\beta = \tfrac{3}{4}K[\nu/\omega D^2] = \tfrac{3}{4}K/S. \tag{4.14}$$

The boundary proximity effect on fluid resistance and fluid inertia would be represented by K and C_M, respectively. For steady Stokes flow about a sphere in an infinite medium $K = 24$. As demonstrated by Stokes (1851), K is a function of S in oscillatory flow. For spheres rolling down a plane boundary at a terminal speed Carty (1957) found $K = 215$. Probably because of blockage effects Chan *et al.* (1974) measured $K = 260$ for the terminal condition of spheres rolling in tubes. The inertia or added-mass coefficient C_M has a value of 0·5 for potential flow about a sphere in an infinite medium, but is a function of S in oscillatory Stokes flow. Experimentally and analytically Garrison & Berklite (1973) determined $C_M = 0{\cdot}67$ for a stationary sphere in contact with a plane boundary. If K and C_M are constant in viscous motion then the ratio of sphere to fluid amplitude is independent of fluid amplitude, as shown by (4.12). The corresponding representation of (4.12) on figures 5 and 6 would be straight lines through the origin. The general curved form of all empirically determined lines on the graphs indicates that the drag law is nonlinear. For the stainless-steel balls the data do tend to approach the origin asymptotically, however. Clearly the data on figures 5 and 6 are inertia dominated for low values of X_{f0}/D and drag dominated for high values.

4.2. *Inviscid flow*

In the case of an ideal fluid motion, for which $\beta = K = 0$, the phase angle $\phi = 0$, and, from (4.12),

$$\frac{X_s}{X_{f0}} = \frac{1+C_M}{\frac{7}{5}\rho_r + C_M} \sin \omega t, \tag{4.15}$$

as derived by Rschevkin (1963).

For the higher values of S for the stainless-steel balls, for which X_{f0}/D is small, the viscous solution (4.12) degenerates to (4.15) because of the small values of β. Therefore, for values of $X_{f0}/D < 6$ the inertia forces dominate and govern the motion. As X_{f0}/D is increased above a value of 6 the nonlinear drag force begins to increase, resulting in values of X_{s0}/X_{f0} increasingly greater than the constant values predicted by (4.12) or (4.15). The straight-line inviscid solution on figure 5 for the stainless-steel balls for $C_M = 0{\cdot}67$ (Garrison & Berklite 1973) suggests that the inertia coefficient could actually be determined solely by the amplitude ratio if the ratio X_{f0}/D is small enough.

4.3. *Nonlinear drag and turbulent flow*

Neither the inviscid solution (4.15) nor the linear viscous solution (4.12) is valid in situations for which the nonlinear drag is a significant force. Houghton (1963) states that complete solutions to the so-called nonlinear Langevin equation (4.10) exist only if the sign of the drag term does not change during the cycle, a fact that is never true for the current investigation. Under certain conditions of oscillating flow in the vertical direction, for which levitation of solid particles in an upward flow is possible (Houghton 1966, 1968; Tunstall & Houghton 1968), exact and approximate solutions can be effected (Houghton 1966, 1968). Numerical solutions are possible with or without these restrictions, of course.

Inasmuch as the actual observed sphere motion X_s was nearly simple harmonic the resultant inertia of the sphere $\frac{7}{5}M_s a_s$, or the right-hand side of (4.9) or (4.10), is known. Let us now define the kinematics of the sphere motion to be

$$X_s = X_{s0}\sin(\omega t-\phi), \tag{4.16}$$

$$V_s = \omega X_{s0}\cos(\omega t-\phi), \tag{4.17}$$

$$a_s = -\omega^2 X_{s0}\sin(\omega t-\phi). \tag{4.18}$$

Equation (4.10) can then be written as

$$(1+C_M)\sin\omega t - C_M\frac{X_{s0}}{X_{f0}}\sin(\omega t-\phi) - \tfrac{3}{4}C_D\frac{X_{f0}}{D}\left[\cos\omega t-\frac{X_{s0}}{X_{f0}}\cos(\omega t-\phi)\right]$$

$$\left|\cos\omega t-\frac{X_{s0}}{X_{f0}}\cos(\omega t-\phi)\right| = \tfrac{7}{5}\rho_r\frac{X_{s0}}{X_{f0}}\sin(\omega t-\phi). \tag{4.19}$$

As the right-hand side of (4.19) is known, the technique of Fourier-averaging, initially applied to forces on piles by Morison *et al.* (1950), and later thoroughly explained by Keulegan & Carpenter (1958), can be employed to determine values of C_M and C_D. If the measured force on a stationary body is F, then the Fourier-averaged force coefficients for a sphere are (Sarpkaya 1975)

$$C_M = \frac{3}{\pi^3}\frac{V_{f0}T}{D}\int_0^{2\pi}\frac{F\sin\theta\,d\theta}{\rho_f V_{f0}^2 D^2}, \tag{4.20}$$

and

$$C_D = -\frac{3}{\pi}\int_0^{2\pi}\frac{F\cos\theta\,d\theta}{\rho_f V_{f0}^2 D^2}, \tag{4.21}$$

where $\theta = 2\pi t/T$. Equations (4.20) and (4.21) are only valid in this form if one motion, either fluid or sphere, is absent. In this study the relative motion complicates the analysis somewhat.

Instead of integrating (4.19) to produce results exactly analogous to (4.20) and (4.21) we express (4.19) in a simpler form

$$-(\tfrac{7}{5}\rho_r+C_M)\frac{X_{s0}}{X_{f0}}\sin(\omega t-\phi)+(1+C_M)\sin\omega t = \tfrac{3}{4}C_D\frac{X_{f0}}{D}$$
$$A^2\cos(\omega t-\alpha)\left|\cos(\omega t-\alpha)\right|, \tag{4.22}$$

where A is proportional to the relative motion,

$$A^2 = 1-2(X_{s0}/X_{f0})\cos\phi+[X_{s0}/X_{f0}]^2, \tag{4.23}$$

and

$$\tan\alpha = -\frac{(X_{s0}/X_{f0})\sin\phi}{1-(X_{s0}/X_{f0})\cos\phi}, \tag{4.24}$$

where α is phase lag between the velocity difference and V_f, as shown on figure 4. For the simple-harmonic water and sphere motion the effective Fourier-averaging is accomplished by (i) multiplying (4.22) by $\sin(\omega t-\alpha)$ and integrating from $t = 0$ to $t = T$, resulting in

$$C_M = \frac{\frac{7}{5}\rho_r(X_{s0}/X_{f0})\cos(\phi-\alpha)-\cos\alpha}{A}. \tag{4.25}$$

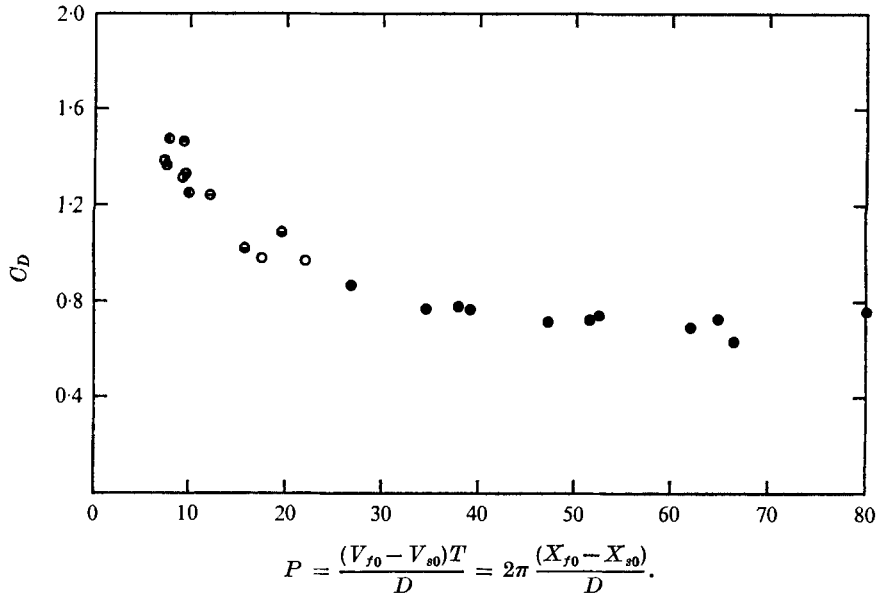

FIGURE 8. Fourier-averaged drag coefficient *vs.* period parameter. ◑, nylon I; ◐, plastic; ⊖, nylon II; ◓, billiard; ◒, glass; ○, blue glass; ●, stainless steel.

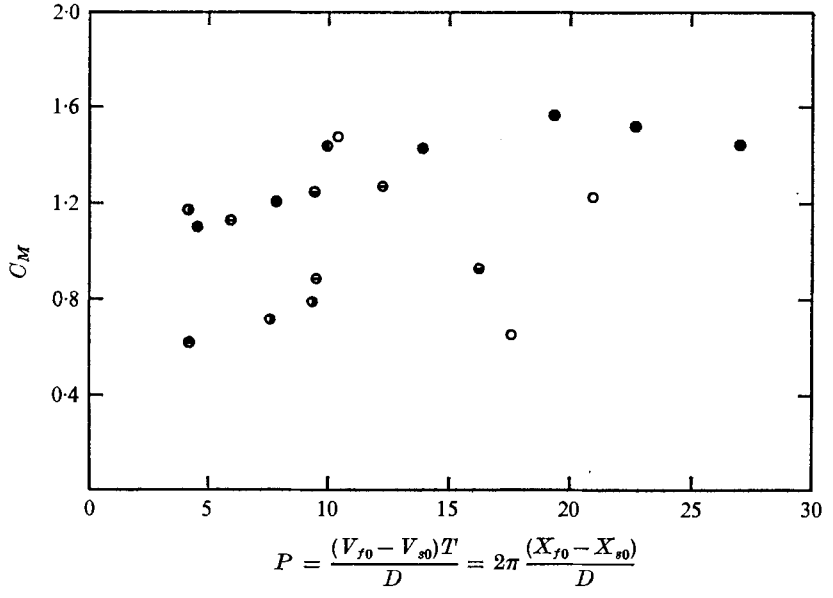

FIGURE 9. Fourier-averaged added-mass moment of inertia coefficient *vs.* period parameter. (Symbols as in figure 8.)

Step (ii) is effected by multiplying (4.22) by $\cos(\omega t-\alpha)$ and integrating over the same interval, in this instance producing the averaged drag coefficient

$$C_D = \tfrac{1}{2}\pi\left[\frac{(\frac{7}{5}\rho_r + C_M)(X_{s0}/X_{f0})\sin(\phi-\alpha)+(1+C_M)\sin\alpha}{A^2(X_{f0}/D)}\right]. \tag{4.26}$$

Theoretically, if the motion can be described by the force equation (4.10) and if the amplitude ratio X_{s0}/X_{f0} and the phase angle ϕ of the motion are determined experimentally (from which A and α are easily calculated), C_M and C_D can be calculated, from (4.25) and (4.26), respectively.

4.4. *Drag coefficient*

As demonstrated by Keulegan & Carpenter (1958) and Sarpkaya (1975) the unsteady drag coefficient can be correlated with a period parameter P in the absence of any Reynolds number effects. The results of this analysis are shown in figure 8 for those tests for which the motion is essentially drag dominated. No data are included for $X_{f0}/D = 3$ because the drag force was too small to permit an accurate determination of C_D. For $P > 30$ the average value of C_D is 0·74, compared with a range of values from 1·2 to 0·8 reported by Carty (1957) for the same Reynolds number range ($820 < (V_{f0}-V_{s0})D/\nu < 8840$ for figure 8). Chan *et al.* (1974) conducted terminal rolling speed tests similar to those of Carty, but found some deviations from his results, probably because they rolled spheres down a tube rather than down a plane boundary. It would be desirable to compare the values of C_D on figure 8 with those determined by Chan *et al.* (1974), but it is not possible by Fourier-averaging as they did not measure the phase angle ϕ during their oscillatory tests. Apparently the wall boundary layer had virtually no effect on the fluid drag over the drag-dominated region ($P > 30$) as C_D remained nearly constant for ratios of the boundary-layer depth of penetration to the sphere diameter from 0·04 ($P = 38$) to 0·12 ($P = 80{\cdot}2$).

4.5. *Added-mass coefficient*

For the lower values of X_{f0}/D and P it is clear from the data on figures 5 and 6 compared with (4.12) or (4.15) that the sphere motion is dominated by the fluid inertia. The Fourier-averaged values of C_M from (4.25) are shown on figure 9 only for $P < 30$. There is considerable scatter because of the sensitivity of C_M to the phase angle ϕ, which could be accurately measured only to several degrees. It is obvious, however, that the rotational fluid effects are influencing the results, as nearly all values of C_M are greater than the theoretical one of 0·67 for a stationary or translating sphere (Garrison & Berklite 1973).

An added-mass moment of inertia exists because of the so-called attached fluid in the sphere boundary-layer. Lamb (1932) determines the magnitude of the torque on an oscillating sphere in an infinite medium by neglecting the convective acceleration terms. The coefficient of the torque term that is proportional to angular acceleration is the added-mass moment of inertia

$$I = 2M_f R^2 \frac{4+(2S)^{\frac{1}{2}}}{4+(2S)^{\frac{1}{2}}+S}. \tag{4.27}$$

For large values of S

$$I = (2\sqrt{2})\, M_f R^2/\sqrt{S}. \tag{4.28}$$

If a coefficient of added-mass moment of inertia C_I is introduced, i.e.

$$I = C_I \tfrac{2}{5} M_f R^2, \tag{4.29}$$

then

$$C_I = (5\sqrt{2})/\sqrt{S}. \tag{4.30}$$

Indeed, the solution for a sphere rotating on a plane boundary at high values of the Reynolds number and Stokes number would not yield the same result as (4.30). An order-of-magnitude effect can be demonstrated, however, by relating (4.29) to the rotational inertia of the sphere itself as the attached fluid can be envisaged as moving with the body. The ratio of (4.29) to $\frac{2}{5}M_s R^2$ is C_I/ρ_r. For the experimental results depicted on figure 9 this ratio varies from 0·03 to 0·17. No attempt was made to incorporate this effect in the determination of C_M because of the lack of a solution for I that includes wall effects.

The difficulty in accurately determining C_M, and to a lesser degree C_D, from (4.25) and (4.26) is partially due to the fact that (4.10) is based upon the following assumptions: (i) the nonlinear drag law has an exponent of two, (ii) the drag force is in phase with the relative velocity, (iii) the inertia or added-mass force is in phase with the relative acceleration between water and sphere, (iv) the history or Basset term is negligible, and (v) the rolling friction force is adequate to prevent sliding. Although the use of a variable drag coefficient during numerical integration was considered, a constant exponent of two in the drag law was employed because of the relatively large Reynolds numbers and the lack of good experimental data. This approach was exercised by Chan *et al.* (1974), but the use of steady-flow (terminal speed) data in an oscillatory flow field is itself questionable. Although the drag force is by definition in phase with the relative acceleration, it is realized that history effects could cause deviations therefrom. Houghton (1966) has demonstrated that a phase lag exists between the added-mass term and the relative acceleration term because of viscous or history effects.

4.6. *History or Basset term*

The importance of the history of the relative acceleration to the rectilinear transient motion of spheres was first recognized by Basset (1910) for low Reynolds number flow. Recently, however, Mockros & Lai (1969) have demonstrated that Stokes theory and the history term as defined by Basset are valid up to much greater terminal Reynolds numbers than would correspond to the limit of the theory for steady flow. For steady-state oscillatory motions in the Stokes or viscous regime the Basset term is well known for a sphere, containing both acceleration- and velocity-dependent terms. For transient motions and non-repetitive oscillatory or pulsatile motions, the Basset term is introduced to account for deviations of the motion from steady state. The importance of the Basset term for oscillatory flows at high Reynolds and Stokes number is not at present known. Odar & Hamilton (1964) calculated the magnitude of the history term from experiment for an oscillating sphere, but only after assuming a value of C_D, which itself was not known *a priori*. Although they demonstrated that the

Basset definition of F_H can be applied to oscillatory flows up to a Reynolds number of 62, it was neglected here because of the much higher values. Al-Taweel & Carley (1971) showed by an approximate analysis that neglect of the history term should cause only a small error if $S \gg 40$. Most authors (notably Chan *et al.* 1974; Houghton 1963, 1966; Tunstall & Houghton 1968) have neglected the Basset term in their analyses of oscillatory and pulsatile flows. It is not unreasonable to speculate that the history term influences the rotational fluid effects more than the translational ones, as discussed earlier.

4.7. *Rolling friction*

Although F_R was eliminated in the derivation of (4.5) its presence is necessary for maintaining rolling of the sphere. If only sliding occurred, as has been conjectured by Goldman *et al.* (1967) and others, the rotating sphere inertia term in (4.2) would be altered. They postulated that a sphere may not even be in direct contact with the boundary because of the high local shear or lubrication force at the point or surface of contact. Analysis of the movement of one marked ball from motion pictures resulted in an identical number of observed and calculated rotations. In fact, all balls were observed to rotate continuously.

For extremely low amplitudes of motion ($X_{f0}/D < 1$) the friction force on the ball would inhibit its motion until a threshold value of X_{f0}/D was attained, beyond which a smooth rolling motion prevailed. This phenomenon was also observed by Chan *et al.* (1974), who reported threshold values of X_{s0} and X_{f0}. Halow (1973) reports that the incipient angle required to initiate rolling of a sphere down an inclined plane is of the order of 5°. Only in the case of the ping-pong ball can it be demonstrated on the basis of Halow's data that the rolling friction force was not adequate to preclude sliding.

5. Numerical analysis

The relative importance of the inertia and drag forces in (4.5) can be demonstrated by numerical integration of (4.10) in terms of V_s. A fourth-order Runge–Kutta technique was employed, using 200 intervals of integration per cycle of oscillation. By starting the integration process with the sphere at rest the desired steady state was only attained once the transients completely decayed, which always occurred after ten cycles. We applied Simpson's rule to integrate V_s for the sphere displacement X_s.

If either C_M or C_D in (4.10) is known then the other one can be optimized by integrating for X_{s0} until the calculated and measured values agree. The optimization in terms of ϕ is not nearly as successful because of the sensitivity of the solution to ϕ.

To optimize for C_D an average value of $C_M = 1{\cdot}2$ from figure 9 is inserted into (4.10). For large values of P the solution is very sensitive to changes in C_D, as shown by the two examples on figure 10. For $P > 30$ all optimized values of C_D in terms of amplitude agreement (figure 10) yield an arithmetic average equal to 0·74, identical to the mean Fourier-averaged value. This means that, for large

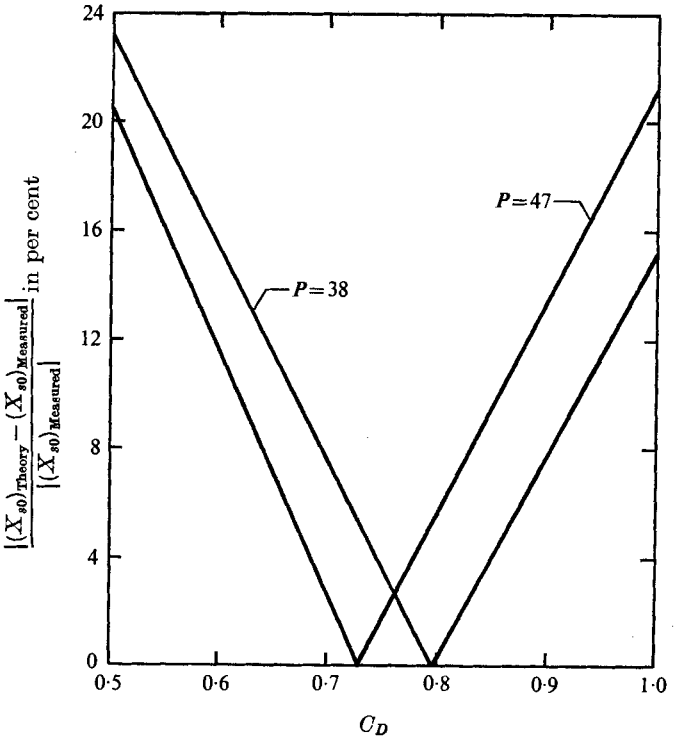

FIGURE 10. Influence of C_D on numerical integration: $\rho_r = 7{\cdot}73$.

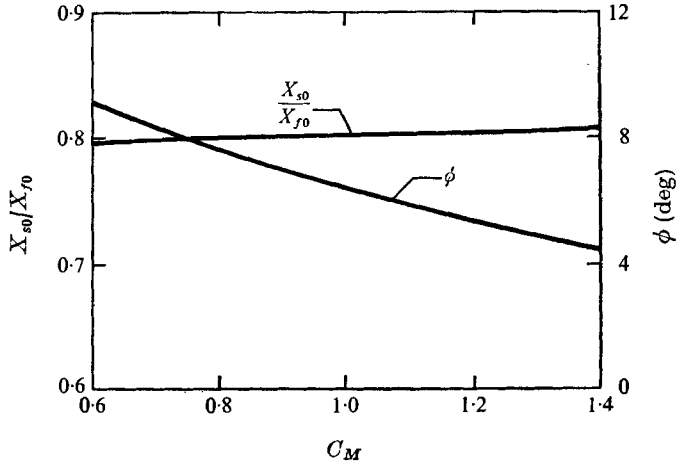

FIGURE 11. Sensitivity of X_{s0}/X_{f0} and ϕ to added-mass coefficient: $\rho_r = 1{\cdot}16$, $P = 7{\cdot}5$.

relative displacement of sphere and fluid, the determination of C_D from (4.26) is not too sensitive to small inaccuracies in ϕ.

We can also employ the numerical integration to perform a sensitivity analysis on either C_M or C_D. Figure 10 in essence exhibits the sensitivity of the motion to changes in C_D. The sensitivity of X_{s0} and ϕ to C_M should depend upon the value

of P. In the inertia-dominated region ($P < 30$) the characteristics of the sphere motion are shown in figure 11 for $0{\cdot}6 < C_M < 1{\cdot}4$. We assumed $C_D = 1{\cdot}45$ from figure 8 for the value of $P = 7{\cdot}5$. It is clear that the phase angle ϕ is more sensitive to changes in C_M than X_{s0}, explaining to some extent the scatter on figure 9, the results of which are based upon Fourier-averaging.

Using $C_M = 1{\cdot}2$ and basing C_D on a best-fit relationship through the data on figure 8 a comparison of the measured values of $(X_{f0} - X_{s0})/D$ *vs.* ρ_r on figure 7 can be effected. The theoretical lines on figure 7 suggest that the amplitude of the sphere motion can be reasonably well predicted from (4.10). Furthermore, the agreement is also good for values of ρ_r for which C_D and C_M were not calculated from (4.20) and (4.21) because there were no data for ϕ.

6. Conclusions

Provided that the friction force between sphere and plane boundary precludes any sliding motion, inertia and drag coefficients can be determined from analysis of relative motion between sphere and fluid. Although both the Stokes number and the Reynolds number were high the drag force is small for sphere displacements less than about six diameters, allowing for the determination of C_M. Under these conditions the added-mass coefficient could even be approximated by Rschevkin's inviscid solution if the ratio of sphere amplitude to fluid amplitude were known. The rotational effect of the fluid causes the inertia coefficient to be higher for rotating spheres ($C_M = 1{\cdot}2$) than for stationary or translating spheres ($C_M = 0{\cdot}67$).

The drag force governs the motion for large values of X_{f0}/D, allowing the determination of C_D. If the period parameter $P > 30$, C_D was determined to be 0·74 from both Fourier-averaging and numerical analysis, a value somewhat lower than for rolling balls in unidirectional motion.

REFERENCES

Al-Taweel, A. M. & Carley, J. F. 1971 Dynamics of single spheres in pulsated, flowing liquids. Part 1. Experimental method and results. Part 2. Modeling and interpretation of results. *Chem. Engng Prog. Symp. Ser.* no. 116, **67**, 114–131.

Basset, A. B. 1910 On the descent of a sphere in a viscous liquid. *Quart. J. Math.* **41**, 369–381.

Brush, L. M., Ho, H.-W. & Yen, B.-C. 1964 Accelerated motion of a sphere in a viscous fluid. *J. Hyd. Division, Proc. A.S.C.E.* **90** (HY1), 149–160.

Carstens, M. R. 1952 Accelerated motion of a spherical particle. *Trans. Am. Geophys. Un.* **33**, 713–721.

Carty, J. J. 1957 Resistance coefficients for spheres on a plane boundary. B.S. thesis, Massachusetts Institute of Technology.

Chan, K. W., Baird, M. H. I. & Round, G. F. 1974 Motion of a solid sphere in a horizontally oscillating liquid. *Chem. Engng Sci.* **29**, 1585–1592.

Dean, W. R. & O'Neill, M. E. 1963 A slow motion of viscous liquid caused by the rotation of a solid sphere. *Mathematika*, **10**, 13–24.

Eagleson, P. S. & Dean, R. G. 1961 Wave-induced motion of bottom sediment particles. *Trans. A.S.C.E.* **126**, 1162–1189.

Faxén, H. 1921 Einwirkung der Gefasswände auf den Widerstand gegen die Bewegung einer kleinen Kugel in einer zähen Flüssigkeit. Dissertation, Uppsala.

GARRISON, C. J. & BERKLITE, R. B. 1973 Impulsive hydrodynamics of submerged rigid bodies. *J. Engng Mech. Div., Proc. A.S.C.E.* **99** (EM1), 99–120.

GOLDMAN, A. J., COX, R. G. & BRENNER, H. 1967 Slow viscous motion of a sphere parallel to a plane wall — I. Motion through a quiescent fluid. *Chem. Engng Sci.* **22**, 637–651.

GRACE, R. A. & CASCIANO, F. M. 1969 Ocean wave forces on a subsurface sphere. *J. Waterways Harbors Div., Proc. A.S.C.E.* **95** (WW3), 291–317.

HALOW, J. S. 1973 Incipient rolling, sliding and suspension of particles in horizontal and inclined turbulent flow. *Chem. Engng Sci.* **28**, 1–12.

HAMILTON, W. S. & LINDELL, J. E. 1971 Fluid force analysis and accelerating sphere tests. *J. Hyd. Div., Proc. A.S.C.E.* **97** (HY6), 805–817.

HAPPEL, J. & BRENNER, H. 1965 *Low Reynolds Number Hydrodynamics.* Prentice-Hall.

HJELMFELT, A. T. & MOCKROS, L. F. 1967 Stokes flow behavior of an accelerating sphere. *J. Engng Mech. Div., Proc. A.S.C.E.* **93** (EM6), 87–102.

HOUGHTON, G. 1963 The behaviour of particles in a sinusoidal velocity field. *Proc. Roy. Soc.* A **272**, 33–43.

HOUGHTON, G. 1966 Particle trajectories and terminal velocities in vertically oscillating fluids. *Can. J. Chem. Engng*, **44**, 90–95.

HOUGHTON, G. 1968 Particle retardation in vertically oscillating fluids. *Can. J. Chem. Engng*, **46**, 79–81.

KEULEGAN, G. H. & CARPENTER, L. H. 1958 Forces on cylinders and plates in an oscillating fluid. *J. Res. Nat. Bur. Stand.* **60**, 423–440.

KÖNIG, W. 1891 Hydrodynamisch – akustische Untersuchungen. *Ann. Phys. Chem.* **42**, 353–370.

LADENBURG, R. 1907 Über den Einfluss von Wänden auf die Bewegung einer Kugel in einer reibenden Flüssigkeit. *Ann. Phys.* **23**, 447–458.

LAMB, H. 1932 *Hydrodynamics.* Dover.

MCNOWN, J. S., LEE, H. M., MCPHERSON, M. B. & ENGEZ, S. M. 1948 *Proc. 7th Int. Cong. Appl. Mech.* pp. 17–29.

MOCKROS, L. F. & LAI, R. Y. S. 1969 Validity of Stokes theory for accelerating spheres. *J. Engng Mech. Div., Proc. A.S.C.E.* **95** (EM3), 629–640.

MORISON, J. R., O'BRIEN, M. P., JOHNSON, J. W. & SCHAAF, S. A. 1950 The force exerted by surface waves on piles. *Petrol. Trans., Am. Inst. Mining Metallurgical Engrs*, **189**, 149–154.

O'BRIEN, M. P. & MORISON, J. R. 1952 The forces exerted by waves on objects. *Trans. Am. Geophys. Un.* **33**, 32–38.

ODAR, F. & HAMILTON, W. S. 1964 Forces on a sphere accelerating in a viscous fluid. *J. Fluid Mech.* **25**, 302–314.

O'NEILL, M. E. 1964 A slow motion of viscous liquid caused by a slowly moving solid sphere. *Mathematika*, **11**, 67–74.

RSCHEVKIN, S. N. 1963 *The Theory of Sound.* Pergamon.

SARPKAYA, T. 1975 Forces on cylinders and spheres in a sinusoidally oscillating fluid. *J. Appl. Mech., Trans. A.S.M.E.* **97**, 32–37.

SHIZGAL, B., GOLDSMITH, H. L. & MASON, S. G. 1965 The flow of suspensions through tubes. Part 4. Oscillatory flow of rigid spheres. *Can. J. Chem. Engng*, **43**, 97–101.

STOKES, G. 1851 On the effect of the internal friction of fluids on the motion of pendulums. *Camb. Phil. Trans.* **9**, 8.

TUNSTALL, E. B. & HOUGHTON, G. 1968 Retardation of falling spheres by hydrodynamic oscillations. *Chem. Engng Sci.* **23**, 1067–1081.

WAGENSCHEIN, M. 1921 Experimentelle Untersuchung über das Mitschwingen einer Kugel in einer schwingenden Flüssigkeits-oder Gasmasse. *Ann. Phys. Ser.* 4, **65**, 461–480.

WAUGH, J. G. & ELLIS, A. T. 1969 Fluid-free-surface proximity effect on a sphere vertically accelerated from rest. *J. Hydronautics* **3** (4), 175–179.